Technical Notes

TECHNICAL NOTES are short manuscripts describing new developments or important results of a preliminary nature. These Notes cannot exceed 6 manuscript pages and 3 figures; a page of text may be substituted for a figure and vice versa. After informal review by the editors, they may be published within a few months of the date of receipt. Style requirements are the same as for regular contributions (see inside back cover).

Navier-Stokes Solution of Complete Turbulent Flow Past Finite Axisymmetric Bodies

Seok Ki Choi* and Ching Jen Chen†
University of Iowa, Iowa City, Iowa 52242

I. Introduction

INCOMPRESSIBLE turbulent flow past axisymmetric bodies of finite length has been the subject of numerous investigations, as it is of major importance in aerodynamics and ship hydrodynamics. An accurate prediction of flowfield near the tail region of axisymmetric bodies is particularly important in ship hydrodynamics since many propellers and appendages are located inside the ship stern boundary layers. The flow evolution in the tail region of axisymmetric bodies is characterized by a rapid growth of boundary layer, a strong viscous-inviscid interaction, and a general reduction in the level of turbulence by streamline curvature and pressure gradient,[1] which is quite different from that in the hull region. These flow features show that the thin boundary-layer approximation is not adequate for describing the flowfield around the tail region and a full analysis of the Navier-Stokes equations is necessary.

In most of the previous studies of Navier-Stokes equations, including those of the present authors,[2] the calculations were started at the middle of the body with inlet flow conditions provided by curve fits of experimental data[3] or simple flat plate correlations.[2] These calculations do not provide the solution of leading-edge interaction and the initial development of the boundary layer near the leading edge. The resulting solutions at the trailing portion are thus dependent on the flow conditions specified at the middle of the body. In order to avoid these deficiencies in the half-body calculations and to obtain the solution of the whole flowfield, the present calculation starts far upstream of the body with flow conditions provided by uniform flow conditions. Numerical solutions of incompressible turbulent flow past the entire finite axisymmetric bodies are obtained using the k-ϵ turbulence model and the wall function method. The complex, physical solution domains are resolved by the use of numerically generated, nonorthogonal, body-fitted coordinates. The governing equations are written in the transformed domain with the cylindrical velocity components as dependent variables. The transformed governing equations are discretized using the finite volume method. The resulting algebraic equations are solved by the solution procedure of SIMPLER (semi-implicit method for pressure linked equation-revised) algorithm.[4] Calculations are performed for four axisymmetric bodies, as shown in Fig. 1, and compared with the available experimental data.[5]

II. Method of Solution

The continuity equation and general form of transport equations for the steady, incompressible flow in a cylindrical coordinate system with the k-ϵ turbulence model can be written as follows:

$$\frac{\partial}{\partial x}(\rho ru) + \frac{\partial}{\partial y}(\rho rv) = 0 \tag{1}$$

$$\frac{\partial}{\partial x}(\rho ru\phi) + \frac{\partial}{\partial y}(\rho rv\phi) = \frac{\partial}{\partial x}\left(r\Gamma_\phi \frac{\partial \phi}{\partial x}\right) + \frac{\partial}{\partial y}\left(r\Gamma_\phi \frac{\partial \phi}{\partial y}\right) + rS_\phi \tag{2}$$

where ϕ represents the general transport variables u, v, k, ϵ; ρ is the density of fluid; (u,v) are the velocity components in (x,y) directions; Γ_ϕ is the effective diffusion coefficient; and S_ϕ denotes the source term for the variable ϕ. The quantities Γ_ϕ and S_ϕ are defined in Table 1. In Table 1, $\mu_{ef} = \mu + \mu_t$, $\mu_t = c_\mu \rho(k^2/\epsilon)$, $c_\mu = 0.09$, $\sigma_\epsilon = 1.3$, $c_{\epsilon 1} = 1.44$, and $c_{\epsilon 2} = 1.92$. The velocity, space, and pressure variables are made dimensionless by the approaching velocity U_∞, the body length L, and ρU_∞^2. The solution domain chosen for the present study is sufficiently large to enclose the complete axisymmetric body. Calculations are started far upstream of the body ($x_u = -2.23$) with inlet flow conditions specified by uniform flow conditions. The solution domain includes, with a dimensionless body length of 1, an upper boundary in the normal direction, $y_u = 2$, and the downstream boundary in the axial direction, $x_d = 9.29$, large enough to capture the entire viscous-inviscid interaction and wake development. The boundary conditions for the problems considered in the present study can be stated as follows: 1) upstream boundary ($x = x_i$) : $u = 1$, $v_x = 0$, $k = k_{in}$, $\epsilon = \epsilon_{in}$; 2) downstream boundary ($x = x_d$) : $u_x = v_x = k_x = \epsilon_x = p_x = 0$; 3) body surface: u, v, k, ϵ specified by wall functions; 4) upper boundary ($y = y_u$) : $u = 1$, $p = 0$, $k_y = \epsilon_y = 0$; and 5) centerline ($y = 0$, $x < 0$, and $x > 1$) : $v = 0$, $u_y = k_y = \epsilon_y = 0$.

The upstream inlet conditions for turbulent quantities k, ϵ are specified by the following uniform conditions, $k_{in} = 1.5(Tu)^2$ and $\epsilon_{in} = c_\mu k_{in}^{3/2}/l_{in}$. The turbulent intensity, $Tu = 0.5\%$ and length scale, $l_{in} = 0.001L$ (L is the body length) are used in the present calculations. In the wall function region, the wall function approach[6] is used. The wall shear stress $\tilde{\tau}_w$ is expressed as a function of the second nodal velocity component parallel to the wall $\tilde{U}_p$ from the inner law

$$U_p^+ = \frac{1}{\kappa} \ln(Ey_p^+) \qquad \text{for } y_p^+ > 11.63$$

The value of ϵ in the near wall cell is obtained from the concept of local equilibrium between production and dissipation of turbulent kinetic energy and is given as $\epsilon_p = c_\mu^{3/4} k_p^{3/2}/(\kappa \delta n)$. The δn is the normal distance from the wall; κ is 0.41.

The boundary-fitted coordinate generation technique is employed for the generation of the numerical grid in the present study. The numerical grids are generated by numerical solution of the Poisson equation with proper specification of grid

Received Aug. 30, 1989; revision received May 21, 1990; accepted for publication May 29, 1990.

*Research Assistant, Department of Mechanical Engineering, Iowa Institute of Hydraulic Research; currently, Research Engineer, Korea Atomic Energy Research Institute, P.O. Box 7, Daeduk-Danji, Tae Jon, Korea.

†Professor and Chaiman, Department of Mechanical Engineering, Iowa Institute of Hydraulic Research. Member AIAA.

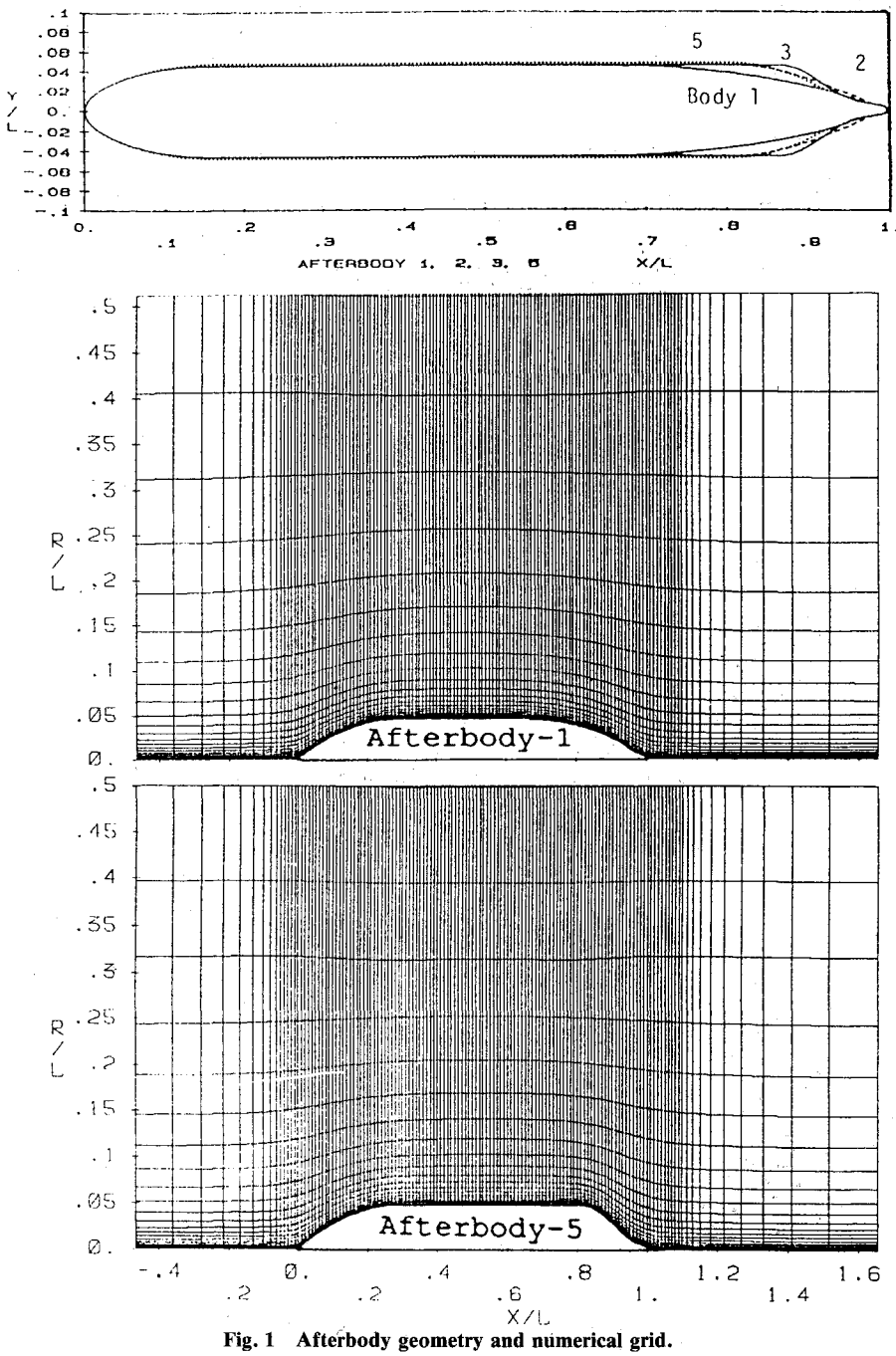

Fig. 1 Afterbody geometry and numerical grid.

control functions. Of the 151 x-directional numerical nodes, 20 nodes are placed upstream of body, 101 nodes are placed on the body, and the remaining 30 nodes are placed in the wake. A partial view of generated numerical grids for afterbodies 1 and 5 is shown in Fig. 1. The solution procedure of the SIMPLER algorithm is employed for all the calculations in the present study.

III. Results and Discussion

Calculations are performed for four axisymmetric bodies of the David Taylor Naval Ship Research and Development Center at $Re = 6.0 \times 10^6$. The extensive experimental data measured by Huang et al.[5] for four different afterbodies, afterbody 1, afterbody 2, afterbody 3, and afterbody 5, provide detailed information on the thick boundary layer and the near wake development. These four bodies shown in Fig. 1 have the same streamlined forebody and parallel middle body, but have different afterbodies. All of these afterbodies have an inflection point and quite dramatic changes in surface

Table 1

ϕ	Γ_ϕ	S_ϕ
u	μ_e	$-\frac{\partial p}{\partial x}+\frac{\partial}{\partial x}\left(\mu_{ef}\frac{\partial u}{\partial x}\right)+\frac{1}{r}\frac{\partial}{\partial y}\left(r\mu_{ef}\frac{\partial v}{\partial y}\right)-\frac{2}{3}\frac{\partial k}{\partial x}$
v	μ_e	$-\frac{\partial p}{\partial y}+\frac{\partial}{\partial x}\left(\mu_{ef}\frac{\partial u}{\partial y}\right)+\frac{1}{r}\frac{\partial}{\partial y}\left(r\mu_{ef}\frac{\partial v}{\partial y}\right)-2\mu_{ef}\frac{v}{r^2}\frac{2}{3}\frac{\partial k}{\partial y}$
k	μ_e	$\mu_e\left[2\left(\frac{\partial u}{\partial x}\right)^2+2\left(\frac{\partial v}{\partial y}\right)^2+2\left(\frac{v}{r}\right)^2+\left(\frac{\partial u}{\partial y}+\frac{\partial v}{\partial x}\right)^2\right]-\rho\epsilon$
ϵ	$u+\frac{\mu_t}{\sigma_\epsilon}$	$c_{\epsilon 1}\mu_e\frac{\epsilon}{k}\left[2\left(\frac{\partial u}{\partial x}\right)^2+2\left(\frac{\partial v}{\partial y}\right)^2+2\left(\frac{u}{r}\right)^2+\left(\frac{\partial u}{\partial y}+\frac{\partial v}{\partial x}\right)^2\right]-c_{\epsilon 2}\rho\frac{\epsilon^2}{k}$

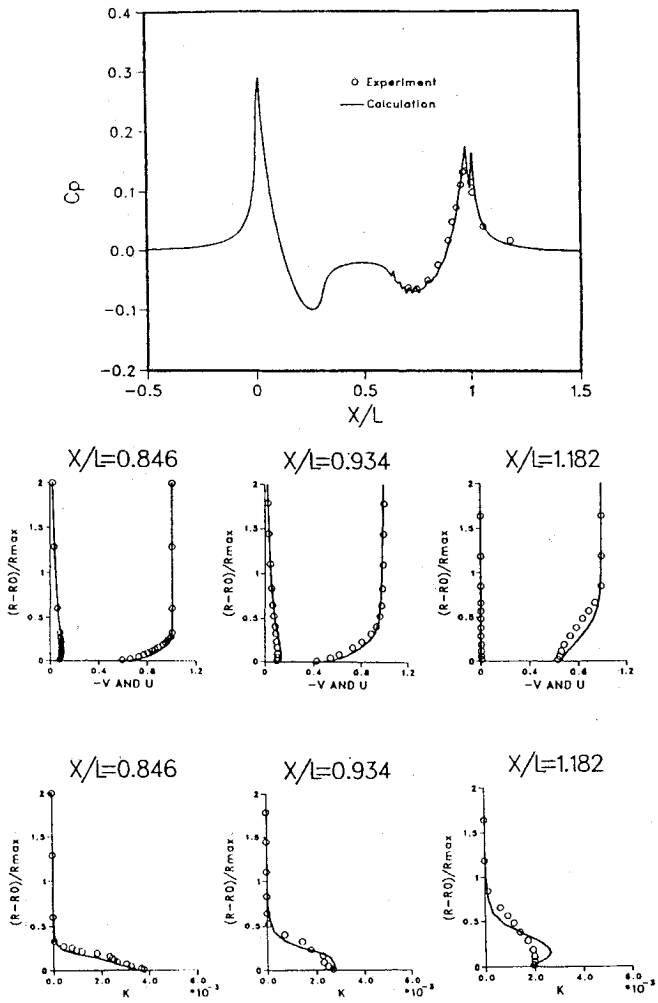

Fig. 2 Turbulent flow past afterbody 1.

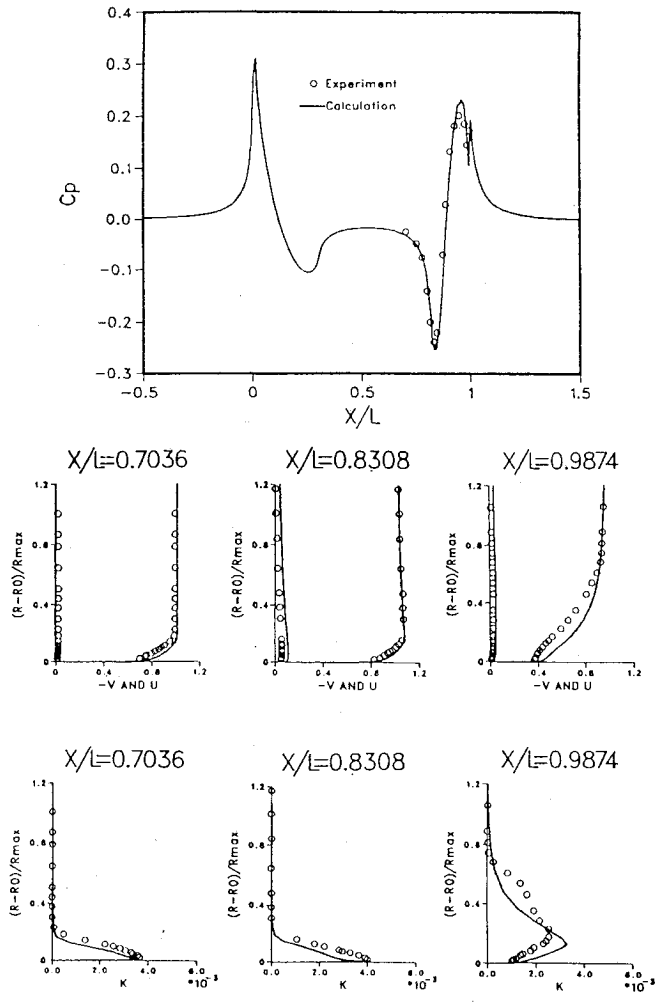

Fig. 3 Turbulent flow past afterbody 5.

curvature, which induce a strong favorable and adverse pressure gradient over the stem region and propeller hub region. The data on these bodies[5] have been widely used in the previous studies for the evaluation of half-body calculation methods and turbulence models. These data are also used in the present study to compare with the results of full-body calculations. The calculation was made for two grid sizes, 151×26 and 151×36. The results from the two grids are found to be approximately the same. Satisfactory convergence was obtained within 300 iterations, RES $< 2 \times 10^{-10}$, although computations are continued to 500 iterations. (RES denotes the mass residue.) In general, the velocity components and pressure field were settled within 100 iterations and the remaining computational efforts were devoted to the development of the far wake.

All subsequent results were obtained with the finer grid (151×36). Figures 2 and 3 show the converged pressure distributions, $Cp = 2\ (p - p_\infty)/(\rho U_\infty^2)$, on the body surface and along the wake centerline for afterbody 1 and 5. The leading- and trailing-edge interactions, as well as the dramatic change of pressure in the regions of stern and hub, are well predicted. The agreement between the predictions and measured data is also good. It is noted that, although the magnitude of pressure at the leading edge is large, it is confined to a small region. The freestream pressure is recovered in the wake in a distance roughly $0.3L$ from the trailing edge of the body. Since the solution domain of the present study extends far beyond this distance, the viscous-inviscid interaction is captured.

Comparisons of the predictions with the measured data for both axial and radial velocity components are also shown in Figs. 2 and 3. The agreement between measured data and the predictions are fairly good except the velocity components are slightly overpredicted in the tail region and in the near wake region due to the neglect of the pressure gradient effect in the turbulence model and in the wall functions. The thickening of the boundary layer in the tail and in the near wake region is well predicted. It is noted that the change of forebody shape does not seriously influence the boundary-layer development in the region of the middle body, thereby, in the stern and wake region. The predictions of turbulent kinetic energy agree fairly well with experimental measurements. Further details of prediction for other afterbodies are given by Chen and Choi.[7]

IV. Conclusions

A calculation method for the solution of the Reynolds averaged, Navier-Stokes equations, together with the k-ϵ turbulence model in a nonorthogonal, body-fitted coordinate system, has been developed and applied to the predictions of the complete turbulent flow past finite axisymmetric bodies. Numerical solutions of a complete turbulent flowfield past axisymmetric bodies that include the leading-edge interaction, boundary-layer development on the body, trailing-edge interaction, and wake development are obtained. The influence of inlet boundary conditions and the location of inlet solution boundary on the solution, which is observed in the previous half-body calculations, is removed in the present calculations.

Overall agreement between measurements and predictions in the present numerical method is demonstrated. For most of the body and near wake region, the pressure and velocity components are fairly well predicted. However, some considerations must be made on the selection of the turbulence model, especially on the near wall treatment, in order to accurately predict the turbulent quantities for the flow involving pressure gradient and streamline curvature effects. The use

of more elaborate wall functions or the introduction of a more advanced turbulence model is needed to properly simulate the flowfield in these situations.

Acknowledgments

This research was partially supported by the Naval Sea System Command AHR Grant N00167-86-K-0019 administered by the Office of Naval Research.

References

[1]Patel, V. C., Nakayama, A., and Damian, R., "Measurements in the Thick Axisymmetric Turbulent Boundary Layer Near the Tail of a Body of Revolution," *Journal of Fluid Mechanics,* Vol. 63, No. 2, 1974, pp. 345-362.

[2]Choi, S. K., and Chen, C. J., "Finite Analytic Numerical Solution of Turbulent Flow Past Axisymmetric Bodies," *Proceedings of the Third International Symposium on Refined Flow Modeling and Turbulence Measurements,* edited by Y. Iwasa, Tokyo, 1988, pp. 121-128.

[3]Muraoka, K., "Calculation of Thick Boundary Layer and Wake of Ships by a Partially Parabolic Method," *Proceedings of the 13th ONR Symposium on Naval Hydrodynamics,* Tokyo, 1980, pp. 601-616.

[4]Patankar, S. V., *Numerical Heat Transfer and Fluid Flow,* McGraw-Hill, New York, 1980.

[5]Huang, T. T., Santelli, N., and Belt, G., "Stern Boundary Layer Flow on Axisymmetric Bodies," *Proceedings of the 12th ONR Symposium on Naval Hydrodynamics,* 1978, pp. 127-157.

[6]Launder, B. E., and Spalding, D. B., "The Numerical Calculation of Turbulent Flows," *Computer Methods in Applied Mechanics and Engineering,* Vol. 3, No. 2, 1974, pp. 269-289.

[7]Chen, C. J., and Choi, S. K., "The Finite Analytic Method and Its Applications—Laminar and Turbulent Flow Past Two Dimensional and Axisymmetric Bodies," Vol. 1, Iowa Inst. of Hydraulic Research, Univ. of Iowa, Iowa City, IA, Rept. 334-I, March 1990.

Flow in the Wake of a Freely Rotatable Cylinder with Splitter Plate

J. M. Cimbala* and S. Garg†
Pennsylvania State University,
University Park, Pennsylvania 16802

Introduction

It is well known[1,2] that a rigidly mounted splitter plate, placed behind a circular cylinder in crossflow, reduces both the cylinder drag and the strength of the shed vortices. Splitter plates have therefore found practical applications, such as suppression of vibration of pitot-static probes in wind and water tunnels. The present work was motivated by the desire to suppress the vibration of a five-hole probe in a water flow, where the oncoming flow direction can be inclined several degrees from the freestream direction, and is not known a priori. In such a case, it was thought that a freely rather than rigidly mounted splitter plate attached to the probe shaft would adjust itself like a weather vane to the changing flow direction. For long plates this was indeed the case, but for shorter plates an unexpected phenomenon was observed. Namely, rather than aligning itself with the flow direction, the splitter plate was observed to rotate to a stable position off axis (on either side of the wake with equal probability). This behavior was first reported by Cimbala et al.,[3] but no explanation of the behavior was given. Their results are summarized in Fig. 1, where stable splitter plate angle θ is plotted as a function of normalized plate length L/D. This angle was found to be independent of Reynolds number for the range tested, which was $5 \times 10^3 < Re < 2 \times 10^4$. As seen, θ decreases continuously with L/D; by $L/D = 5$ the splitter plate, although free to rotate, remains at $\theta = 0$, i.e., parallel to the flow direction.

Recently Xu et al.[4] performed some numerical experiments in an attempt to explain this behavior. Their results show a critical Reynolds number below which the splitter plate is stable at the line of symmetry and above which a symmetry-breaking bifurcation appears. Above the critical Reynolds number, the separation bubble in the cylinder's wake leads to a nonzero unstable moment about the axis, forcing the splitter plate assembly to rotate to a stable position where the moment is zero. Their calculations show that stable splitter plate angle θ decreases with L/D, which agrees qualitatively with the experiments of Cimbala et al.[3] Unfortunately, the maximum Reynolds number of the calculations was 50, far below that of the experiments, and quantitative comparisons are not possible. Nevertheless, the explanation of Xu et al.[4] is considered adequate even for the high Reynolds number experiments. Namely, the time-averaged mean flow in the separated near wake of the cylinder is similar to the steady separation bubble of low Reynolds numbers and imposes an unstable moment on the splitter plate, causing it to migrate to its stable off-axis position. Reynolds number independence implies that the moment is caused primarily by pressure rather than viscous forces. This has been verified[5] in our laboratory by placing a shroud around the front portion of the cylinder, effectively removing the viscous moment. These data are also included in Fig. 1; the shroud has no effect on θ.

Presented here are smoke-wire visualizations and shedding frequency measurements in the wake of the cylinder/splitter plate body. Comparisons are made between the plain cylinder, the cylinder with a splitter plate rigidly fixed at $\theta = 0$ deg, and the freely rotatable cylinder/splitter plate body.

Results and Discussion

The experiments were conducted in a wind tunnel, using a two-dimensional circular cylinder with a splitter plate attached. The cylinder/splitter plate combination could be made freely rotatable about the longitudinal axis of the cylinder, which was always mounted normal to the freestream. Both horizontal and vertical orientations were tested; gravity does not play a role in the observed phenomenon. Further details of the experiment can be found in Ref. 5. Figure 2 compares

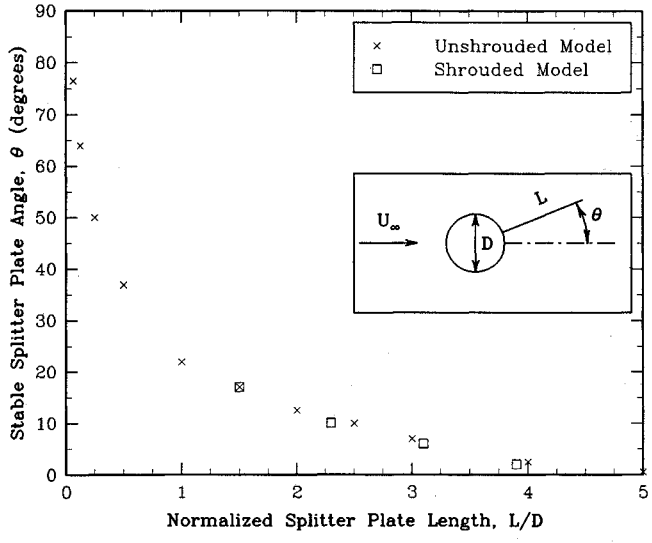

Fig. 1 Variation of stable splitter plate angle with splitter plate length for a freely rotatable cylinder/splitter plate body at Reynolds numbers between 5×10^3 and 2×10^4.

Received May 14, 1990; revision received June 13, 1990; accepted for publication June 13, 1990.

*Associate Professor, Department of Mechanical Engineering. Member AIAA.

†Graduate Assistant, Department of Mechanical Engineering.